Static and Dynamic Model Update of an Inflatable/Rigidizable Torus Structure

Lucas G. Horta and Mercedes C. Reaves
NASA Langley Research Center, Hampton, Virginia, 23681-2199
e-mail – lucas.g.horta@nasa.gov, mercedes.c.reaves@nasa.gov
Telephone number 757-864-1306

The present work addresses the development of an experimental and computational procedure for validating finite element models. A torus structure, part of an inflatable/rigidizable Hexapod, is used to demonstrate the approach. Because of fabrication, materials, and geometric uncertainties, a statistical approach combined with optimization is used to modify key model parameters. Static test results are used to update stiffness parameters and dynamic test results are used to update the mass distribution. Updated parameters are computed using gradient and non-gradient based optimization algorithms. Results show significant improvements in model predictions after parameters are updated. Lessons learned in the areas of test procedures, modeling approaches, and uncertainties quantification are presented.

A Procedure for Static and Dynamic Model Update of Finite Element Models: Application to an Inflated/Rigidized Torus

Lucas G. Horta, Mercedes C. Reaves,
NASA Langley Research Center
Hampton, VA 23681

and Jiann-Shiun Lew
Tennessee State University, Nashville, TN 37203

Abstract

In industry and in government, finite element analysis has become the standard high fidelity method for predicting structural performance of systems. Although computer programs can handle large dimensional problems well, uncertainty in the parameters used in the finite element models often results in a mismatch between pre-test predictions and actual test results. Often, uncertainty in these model parameters and even the selected modeling approach is not captured during model development, which then makes the model update task that much more challenging for the engineer. Although research in model updating has produced hundreds of papers, a universal approach still does not exist, partially because, from a mathematical viewpoint, model updating is an ill posed problem with no single solution. Despite these challenges and limitations, engineers must provide accurate structural models to aid in making decisions regarding systems failure, safety, control system adequacy, etc. This paper presents a model update procedure that uses parameter uncertainty propagation to evaluate the likelihood that a parameter set exists, and expresses this likelihood in terms of confidence intervals for static problems and principal components bounds for dynamic problems. To compute a reconciling solution parameter updates are obtained by minimizing a quadratic performance criterion using a genetic optimization algorithm. Because statistical analysis of complicated systems is computationally intensive and time consuming, a representative set of high fidelity solutions is used to create a Moving Least Squares (MLS) response surface model that is then used for statistical analysis and optimization. MLS provides the means to capture high fidelity solutions from structural analyses into response surface models. To provide the data to demonstrate the update procedure, limited static and dynamic tests are conducted using an inflated/rigidized torus structure. Details on testing, analysis, computation tools, uncertainty bounds, and update results are all presented.

Introduction

A significant part of this effort deals with the problem of model update to reconcile differences between test and analysis. This, of course, is an area that has been investigated thoroughly by researchers in the US and abroad. Although model update has been a very prolific area of research, no single technique is universally accepted and, from a deterministic viewpoint, one might concur with *Avitabile* [2000] when he referred to it as a problem with endless possibilities. For years, the commercially available model update tools relied upon sensitivity information to judge the relative importance of parameters and to assist in making model changes. *Friswell* [1995] discusses many of the

conventional sensitivity based approaches, some of which are implemented in commercial tools. These tools, in the hands of experienced engineers, provide heuristic approaches for model updating that can work very well in reconciling differences between test and analysis; however, they also often suggest unrealistic parameter changes and give the engineer very little insight into the probabilistic nature of the problem. It is this probabilistic aspect of the problem that has prompted extensive research aimed at addressing uncertainty, with noteworthy contributions from *Hasselman* et al., [1994]; *Herendeen* et al., [1998]; Alvin, [1997]; and *Farhat and Hemez*, [1993]. *Hasselman* discussed the propagation of parameter uncertainty in frequency response calculations and presented various approaches to handle the variability of response values near dynamic resonance conditions. *Herendeen* et al., [1998] discussed a mathematical procedure using multi-disciplinary optimization to conduct analysis/test correlation studies of frequency response data. *Alvin* [1997] extended a procedure developed by *Farhat and Hemez,* [1993] to improve convergence and to incorporate uncertainty information into the estimation process, taking full advantage of the model structure and sensitivity. To their credit, very high dimensional problems have been updated successfully using these techniques. However, in the end, the question about realism of updated parameters is still unanswered and left to the individual engineer to assess based on his/her experience. To properly address this question one would need to exploit the work that *Montgomery* [2001] has done in terms of Design of Experiments and Analysis of Variance as a means to judge parameter adequacy. In the work of *Uebelhart*, [2005] tools from the Design of Experiments methodology are heavily relied upon for uncertainty quantification and parameter selection. Regardless of the parameter selection approach, engineering judgment will always play a key role and these tools exist to guide the analyst.

In the computational fluid dynamics (CFD) area, work by *Oberkampf* [2003] and *Roach* [1998] is leading the verification and validation of mathematical models effort. In this area, techniques for systematic assessments of model adequacy and uncertainty quantification have been established along with standards and a common model update language. Unfortunately, these efforts and the associated methods are just now slowly migrating to other disciplines (see *Thacker* [2005], for example). The principles for model verification and validation set forth by the CFD community are applicable to many other disciplines but the metrics for assessment need to be modified. Using their terminology, the work presented here is primarily a model calibration effort.

Fundamental to the success of any model update effort is a clear understanding of the ability of a particular model to predict the observed behavior, even when the observed behavior is uncertain. With this in mind, the approach here is focused primarily on the parameter uncertainty propagation and quantification, as opposed to a search for a specific reconciling solution. The process set forth follows a two-step approach that first uses parameter uncertainty propagation to evaluate uncertainty bounds and to gage the ability of the model to explain the observed behavior. After completing this step, one is able to state, in a probabilistic sense, the likelihood that a parameter set exists that explains the observed behavior. Parameter variances, single and multi-parameter, are computed using response surface models to determine output statistics and confidence

intervals. In contrast to static problems, dynamic problems use Frequency Response Functions (FRF) directly. In addition, to establish uncertainty bounds, discrete probabilities of maximum/minimum principal components as a function of frequency are used to determine the likelihood that a solution exists that reconciles the test FRF with analysis. To obtain a parameter set that reconciles the model with test, nonlinear optimization using the quadratic objective function proposed in *Hasselman* et. al., 1994 is used. Since nonlinear optimization is computationally intensive, a moving least squares (MLS) response surface, developed by *Krishnamurthy* [2002], is created from finite element solutions and used during optimization. Similarly, for dynamic problems, MLS is used not only to predict frequency response functions but also to search for an optimum solution. Although *Zhang* [2005] proposed the use of a conventional response surface, MLS is used in this work because it allows accurate prediction of frequency response functions with relatively small dimensional response surface models. Another aspect of this work that is slightly different from other published work is the use of Principal Components (PC) in the probabilistic assessment of bounds for dynamic problems. *Hassleman* [2002] also used PC in a procedure he calls a PC-based statistical energy analysis for generic uncertainty quantification. Our approach is very similar with the addition of PC maximum and minimum bounds. By using PC bounds, this enables assessments of the probability of finding a solution before any optimization work is done. After the probability of finding a solution is established, optimization with a quadratic error function is used to find a solution to reconcile the model prediction with test. Although the solution itself is often perceived as the most important outcome of the update process from an engineering viewpoint, it should be recognized that it is only one possible solution to the problem; the proposed update solution is infinitely more valuable to the engineer when it is accompanied by some measure of confidence that the resulting parameter values are probable, which are established in this method. In our view, the most valuable aspect of this effort is a set of MATLAB script files that allow users to apply these techniques to a variety of linear or nonlinear problems. Future work needs to incorporate a probabilistic performance metric.

Work cited in this area is not intended to be a comprehensive list of work, but rather examples of activities that guided some of the thinking behind the methods developed and described in this paper.

Problem Formulation

Any model update procedure begins with an initial assessment of the model adequacy and its intended use. For example, if the model is developed to predict loads, detailed modeling of critical loaded regions must be included. On the other hand, if the model is developed to support control design, critical structural modes are measured and calibrated against the model. The intended use of the model determines the type of test and update procedure to follow. In this work, the update procedure is developed such that static deformations as well as improved input/output models for control design can be handled within the same computational framework. Although the approaches are computationally similar, the type of data used and the parameter selection process is different. In the following sections, the model update process is described starting with the parameter

selection process and uncertainty propagation, optimization problem formulation, and the development of response surface models.

Parameter Selection Process and Uncertainty Propagation

Parameter selection for model update is perhaps the most difficult and important task the analyst has to undertake. It is at this stage where engineering judgment and good understanding of modeling deficiencies come into play. After judicious selection of an initial parameter set, probabilistic analysis is used to assess the likelihood that the measured responses can be adequately captured by model predictions. In contrast to parameter selection approaches that use sensitivity matrices exclusively, here a "Monte Carlo" like simulation is used to conduct confidence interval calculations. Unlike conventional Monte Carlo simulations that require thousands of function evaluations, this simulation phase requires fewer function evaluations by concentrating on high probability intervals. In the end, these uncertainty interval calculations are aimed at determining how probable it is for our model to explain the measured response. Although this is a computationally intensive task, the results are critical not only to answer the question about probability but also to provide the data that is ultimately used to update parameters.

The parameter selection process can be divided into four steps: first, a parameter set is selected using engineering judgment; second, uncertainties for these parameters are prescribed in terms of probability distribution functions; third, statistical analysis of the output probability and bounds is computed; and finally an assessment of the probability that our model will capture the measured response is established. Of course, in the event that the initial parameter set is inappropriate, a modified set is selected and the process is repeated. Probability assessments are all based on discrete probabilities computed using a prescribed number of parameter variations. For example, using 100 parameter variations the discrete probability of observing a particular output set is simply 1/100. An output set includes all outputs predicted with a given parameter vector. Our goal is to select a parameter set that makes the probability of capturing the measured response high, otherwise any subsequent attempts to update parameters is likely to have a low probability of explaining the test results. After establishing that a solution that reconciles test with analysis exists within the range space of the parameter set selected the next step is to find such a solution using optimization. The next section describes the problem formulation for optimization.

Optimization Problem Formulation

In contrast to conventional probabilistic analysis where parameters are selected to minimize the probability of exceeding some metric (e.g. stress, deflection, acceleration level), a deterministic criterion is used instead to quantify error differences between test and analysis. To reconcile differences between test and analysis a commonly used performance metric (objective function) is:

$$F(v,u) = (v_o - v)^T S_{vv}^{-1}(v_0 - v) + \sum_{i=1}^{r}(u_t^i - u^i)^T S_{uu}^{-1}(u_t^i - u^i) \quad (1)$$

Where $u^i \in \mathbb{R}^{q\times 1}$ is a vector of predicted responses corresponding to the parameter vector $v \in \mathbb{R}^{m\times 1}$ and the i^{th} input load; $v_o \in \mathbb{R}^{m\times 1}$ is a vector containing the nominal parameter values; $u_t^i \in \mathbb{R}^{q\times 1}$ is a vector of measured responses; $S_{vv} \in \mathbb{R}^{m\times m}$ and $S_{uu} \in \mathbb{R}^{q\times q}$ are weighting matrices, *r* is the number of inputs, *m* is the number of parameters, and *q* is the number of outputs. This form of the objective function, used extensively by *Herendeen* [1998] and others, penalizes both prediction errors and parameter changes from the nominal values. When the weighting matrices are replaced by covariance matrices in the optimization procedure, this solution approaches that of a Bayesian estimation process in the limit as the population tends to infinity.

When reconciling differences between test and analysis FRF for dynamic problems the performance metric in Eq. (1) must be modified as follows:

$$\begin{aligned} F(v,u) &= (v_0 - v)^T S_{vv}^{-1}(v_0 - v) + \\ &\sum_{i=1}^{r} tr\{(u_t^i(j\omega) - u^i(j\omega))^T S_{uu}^{-1}(j\omega)(u_t^i(j\omega) - u^i(j\omega))\} \end{aligned} \tag{2}$$

In this case $u_t^i \in \mathbb{C}^{N_f\times q}$ is a matrix with the complex coefficients of the measured FRF for the i^{th} input, $u^i \in \mathbb{C}^{N_f\times q}$ is a matrix with the predicted FRF, $S_{uu} \in \mathbb{C}^{N_f\times N_f}$ is a frequency weighting matrix, N_f is the number of spectral lines in the FRF, and ω is the frequency.

Solutions to equations (1) and (2) can be obtained using both conventional gradient based optimization and more exhaustive search algorithms such as genetic algorithms. Results for this paper use the genetic algorithm by *Chipperfield* [1994].

Depending on the type of structure being analyzed, FEM models and their solutions can be computationally intensive. Since the parameter selection process relies on statistical analysis of the response data, it is important that no FEM solution is wasted. A way to capture information from every computed solution, as parameters are changed, is to use response surface models. For this purpose, the Moving Least Square algorithm is selected and briefly summarized in the following section.

Moving Least Squares Response Surface Formulation

A response surface model is a mathematical representation of input variables (variables that the user controls) and output variables (dependent variables). Many papers have been published on response surface techniques but the approach selected and used is from *Krishnamurthy* [2002]. This method was selected over conventional techniques because it uses a spatially dependent model representation that is more accurate. In this formulation the input/output relationship is given in parametric form as:

$$\begin{aligned} \hat{U} &= p^T A^{-1} B U \\ A &\triangleq \sum_{i=1}^{N} w_i(v)\, p(v_i)\, p_i^T(v_i) \\ B &\triangleq \sum_{i=1}^{N} w_i(v)\, p(v_i) \\ P^T &\triangleq \begin{bmatrix} p(v_1) & p(v_2) & \cdots & p(v_N) \end{bmatrix} \end{aligned} \tag{3}$$

where $\hat{U} \in \mathbb{C}^{1\times qN}$ is vector of predictions, $U \in \mathbb{C}^{1\times qN}$ is a vector of responses (often obtained from high fidelity analyses and stacked row-wise), v_i is the i^{th} parameter vector from a sample population whereas v is a variable representing the parameters, N is the population size, $w_i(v)$ is a user-defined function that weights the proximity of other parameter vectors on the response surface, and $p(v)$ is a set of basis functions. *Krishnamurthy* [2002] provides several weighting functions to handle problems with different continuity requirements given as a function of the proximity radius, where the radius is defined as $\rho = \|v_i - v\|_2 / l$ and l is often a user defined distance. In our implementation of MLS the proximity radius is computed directly from data using a quadratic search to minimize the error between the data and the response surface prediction. Also to avoid having a catalog of weighting functions for problems with different continuity requirements, the $\sin c(\rho) = \sin(\rho)/\rho$ function is used instead. Since the *sinc* function looks like a hat, raising it to some power just sharpens it and therefore changes the number of neighboring points "under the hat"; in our implementation it is arbitrarily raised to the fifth power. To report the quality of the MLS model the average error is computed as $e = sum\,|U - \hat{U}\,| / qN$, where sum is the over all the components of the error vector, and reported for the cases discussed later.

Sampling techniques are critical to the success of response surface techniques and statistical analysis. For this work, a *Hammersly* [1960] sampling technique is used to generate all parameter variations. *Hammersly* sampling has proven to have good convergence behavior of statistical quantities (mean and variance) and excellent spatial coverage for multi-dimensional problems.

Description of Test Structure

NASA and Tennessee State University (TSU) have been working jointly on dynamics and controls of an inflatable/rigidizable hexapod, shown in Figure 1. Since structures like this appear often as part of telescope assemblies, NASA is particularly interested in it for space applications. In spite of an initial effort to develop a FEM for control design, this initial model missed critical structural modes. Instead of attempting to update the full hexapod model, the torus section shown in Figure 2 is used to evaluate the model update procedure. The torus consists of twelve 0.0181 m diameter tubes arranged to form a 3.72 m circle with urethane composite joints connecting the tubes**.** Tubes are fabricated using a thermoplastic graphite epoxy woven composite, developed by ILC-Dover, Inc, that decreases its modulus when heated above the glass transition temperature, allowing the material to be flattened folded or rolled into a smaller volume. For this application the tubes are rigidized prior to assembly and connected using joints cast from glass filled urethane. Each tube has joints glued on each side that are fastened with bolts to form the torus shape.

Experimental Results

When studying ways to update models where static and dynamic test data are used, the type and quality of data collected is as important as the update process itself. Because the torus structure is built from extremely lightweight materials, testing requires special non-contacting sensing techniques. The following sections describe the test efforts.

Static Test of Torus Section

Static tests results are important to calibrate stiffness parameters and loads, however, to conduct tests with predictable boundary and loading conditions is a challenge. The static test configuration shown in the photograph of Figure 3 is the final configuration selected after a number of configuration changes (see *Berger* [2004]). In this configuration shown in Figure 4, the torus is in a horizontal position and supported at three locations 120 degrees apart. Support 1 consists of an aluminum bracket rigidly connected to three points on the urethane joint flange on one end and fixed to the floor on the other end, with all rotations fixed. Steel blocks provide support at locations 2 and 3 to simulate pinned-pinned conditions. A point load is applied at one of the urethane joints in the vertical direction and displacement measurements are taken at 24 target locations (numbering shown in Figure 4) using the laser displacement sensor (Keyence model LK-503) shown in Figure 5. To collect data from all points, the displacement sensor is moved manually from one location to the next while the load is applied and removed for each individual measurement. Output from the laser sensor is measured on a voltmeter and recorded manually. Data collected from two identical load cases yielded an average difference between the measurements of 0.112 mm, which coincides with the reported instrument resolution (0.1 mm) and also observed during calibration. With a load of 42.1 N the deflection measurements at locations 5, 13 and 21 (support locations) fall below the instrument resolution and are not used in the update process.

Dynamic Test of Torus Section

Dynamic testing is conducted with the torus suspended horizontally, as shown in Figure 6. A spring /cable suspension system is designed such that all six suspensions frequencies are below the first torus frequency. An electromagnetic shaker is used to impart forces through a force gage attached to a Nylon stinger (3/32" diameter). Eighteen retro reflective targets are placed on the perimeter of the torus, Figure 7, and are oriented at a 45 degrees angle from the horizontal plane. These targets, placed coincident with nodes in the FEM, are there to provide an adequate reflective surface for an Ometron VH300+ Laser Doppler Vibrometer (LDV) used to measure velocity. To recover the location and orientation of each measured velocity vector, the LDV location and orientation with respect to the FEM coordinate system is recorded for post-processing the data into components along the X,Y,Z of the global coordinate system. Although laborious, this process provides velocity components at arbitrary angles that would otherwise be difficult to measure. Note that the X-Y plane is horizontal and the Z direction is along the gravity vector. For excitation, a sinusoidal sweep provides energy in the 3 to 110 Hz frequency range while the FRF data are collected at each target location. Three independent modal surveys are conducted with the shaker moved to three different locations; shaker locations 1 and 2 are along Z-axis and shaker location 3 is at 90 degrees from vertical.

Finite Element Model Description

An initial FEM model of the hexapod, previously developed and reported in *Adetona* [2003], uses equivalent beam properties to model most of the structure. Correlation of the finite element model with dynamic data brought up more questions than answers, and prompted a model refinement investigation following a more incremental approach using

component data, starting with the torus. Here, a FEM model of the torus is created from CAD geometry using EDS-IDEAS and then exported to MSC/NASTRAN for analysis. A schematic of the FEM shown in Figure 8 contains 6,897 grid points with 41,382 degrees of freedom. Two-dimensional plate elements (CQUAD) are used to model the tube/joint assemblies. For the tubes, woven composite material properties are modeled using orthotropic material properties cards (MAT8). Tube material properties are derived using the fiber and resin properties in the rule of mixtures to calculate uni-directional composite properties. Through standard laminate codes, *Vinson* [1998] for example, the 'effective single ply properties' of the woven composite are determined. Similarly, the glass filled urethane joint properties are calculated using the rule of mixtures and are then input into the FEM as linear isotropic material properties (MAT1). Shell property cards (PSHELL) are used to specify plate thicknesses throughout the structure; however, inflated/rigidized structures do not exhibit the same thickness uniformity as conventional metal structures. Although tube thicknesses throughout the structure vary, in our study a uniform tube nominal thickness of 0.000356 *m* is used. Thicknesses of the joints also vary but the nominal value for the flange is 0.01016 *m*, the inner joint is 0.00634 *m*, and the outer joint is 0.00317 *m*. Other components like the spring/cable suspension system are incorporated using scalar spring elements (CELAS2) with stiffness of K1=3745 *N/m*, K2=3667.2 *N/m*, K3=3726 *N/m* whereas bar elements (CBAR) are used for the 1.6 mm diameter steel cable. Finally, boundary conditions are modeled using single-point constraints and selected grid points are defined to map the measurements and inputs locations.

Computational Framework

One of our goals is to develop computational tools that are independent of specific FEM programs to allow engineers to use our tools with the FEM solvers with which they have the most familiarity. Since MSC/NASTRAN is commonly used at NASA Langley, the most flexible approach is to manipulate the NASTRAN bulk data file structure directly. For cases where a different structural analysis program is used only the input/output interface to the program needs to change. Figure 9 shows a data flow diagram implemented using MATLAB Script files. These script files modify the NASTRAN bulk data for statistical analyses and also read NASTRAN output punch files. Since all the results are stored within the MATLAB environment, all the MATLAB toolboxes are available for use.

Discussion of Results

Static Model Update Results

Selection of parameters for model update is the most important step in the update process. Although researchers have proposed localization approaches to pinpoint problem areas in the model, often times engineering judgment, knowledge of parameter uncertainties, and sensitivity information seems to work best. In our problem, parameter uncertainties in the torus finite element model are associated with material properties and fabrication. Specifically, laminate thickness variation along the torus tubes, irregular cross-sectional areas, uncertainties in the material properties of the woven graphite/epoxy composite and urethane joints, tube geometry after rigidization, and the stiffness of the

glue tube/joint connection are all questionable. Therefore, all these uncertainty sources must be considered during uncertainty quantification.

Sensitivity information is often used during parameter selection but it is not sufficient by itself. For example, it is possible to come up with a very sensitive set of parameters that are unable to explain observed behavior. For probabilistic analysis, confidence intervals, analysis of variance, and principal components are key tools for parameter selection. To avoid biasing the solution, the least informative probability distribution (uniform distribution) is assigned to each parameter along with judiciously selected upper and lower bounds. With this selection the reasonableness of the parameter variations is assured.

Analysis of variance is the primary tool used in the parameter selection phase for static problems. To conduct the analysis of variance for the torus problem, an MLS response surface model (18 variables and order 2) is created using 300 NASTRAN predictions of the output displacement with the parameters in Table 1 distributed uniformly between the bounds under a 42.1 N applied load. For this case the computed MLS average error is $1\times10^{-7}m$. From the 300 NASTRAN solutions, one can compute the mean, variance, and confidence interval for each sensor output when all parameters are simultaneously varied; this will be referred to as the total variation. To study the individual parameter contribution to the total displacement variation, the MLS model is used instead of NASTRAN to generate simulated displacements by varying one parameter while all others are held at their nominal value. This allows one to compute the individual parameter contribution to the displacement mean, variance, and corresponding confidence interval. In all subsequent results, a 95% confidence interval is used during this parameter selection process. Note that if the model is to explain the measured response, the 95 % confidence interval from the total displacement variation should contain the mean value of the measured displacement. Furthermore, if an individual parameter uncertainty contributes to a particular output variation, the individual parameter confidence interval must also be within the 95 % interval of the total variation. In other words, if the total displacement variation using all parameters is $\mu \pm 2\sigma$, for the 95% confidence interval, individual parameter confidence intervals must also be within this interval. With 18 parameters and 21 outputs, it is difficult to examine all the data at once to make decisions about the adequacy of the selected parameters. A way to portray all this information in one plot is shown in Figure 10. Along the abscissa is the parameter number, in the same order as in Table 1, the ordinate indicates the output number (shown in Figure 4) and at the intersection of those two is a colored square sized according to the total normalized displacement variance. The normalized variance is simply the sampled variance divided by $2\sigma_{\max}$ (computed value 0.00065 m) where $\sigma_{\max}$ is the maximum total variance from all the data. Hence, a filled square corresponds to a $4\sigma_{\max}$ variation. To assess the contribution from individual parameters, let the individual parameter interval be defined as $\mu_p \pm 2\sigma_p$ and the normalized interval be defined as $(\mu_p - \mu \pm 2\sigma_p)/2\sigma_{\max}$ and plotted in Figure 11 as black-line squares. Since predicted mean displacements are not plotted, the color green is used to indicate that the measured displacement is captured by the model predicted interval; a red color indicates that measurement is out of the 95 % predicted interval. Although hard to see, output 11 is the only one red. The column to the

right of Figure 10 (lined up with the output number) shows the predicted mean values in meters for the 42.1 N load. From Figure 10 several observations should be made; all the selected parameters contribute significantly to outputs 1-3 and 20-21 variances, but other output locations only show small total variances, making the impact of parameter changes at those locations hard to detect and therefore hard to correct. More importantly, for certain outputs such as number 11, the total variation predicted with our model does not capture test results indicating that this parameter set is unable to reconcile the solution.

After selecting a set of parameters for update, a genetic algorithm is used with the MLS model to find a set of parameters to reconcile test data with analysis. The same response surface model generated and used for the analysis of variance is also used to minimize the objective function defined in Eq. (1).

Figure 11 shows NASTRAN predictions of the static displacements and Figure 12 shows the measured mean displacements (solid blue line) from two tests. Sensor numbering starts at 1 where the load is applied and increases around the circumference, as shown in Figure 4. Hence, in Figure 12, points 1 and 24 are adjacent. With only two measurement sets, a *t*-distribution is used to compute the 95 % confidence interval that is marked with the plus symbols in Figure 12. This experimentally computed variance is used in Eq. (1) to define the weighting S_{uu} matrix while S_{vv}^{-1} is set to 1×10^{-12}, to keep from biasing the solution towards the nominal value. The dashed line corresponds to displacements using the updated set of parameters and the dotted line corresponds to displacements using the nominal values. All predictions are computed using the MLS model. Figure 13 graphically shows the parameter changes from the mean after optimization with the length of the vertical lines indicating allowed parameter variation. Black rectangles correspond to a decreased in value whereas white rectangles are increased values. For example, the first parameter is reduced from 1.1 of the mean to less that 0.8. Mean values are printed across the bottom of the figure for reference. Finally, note that parameter 12 (tube shear modulus 34) is practically unchanged after optimization.

Dynamic Model Update Results

As described earlier, dynamic frequency response functions are measured using a laser vibrometer at 18 locations on the torus. Unfortunately, the data collection process is time consuming (about 5 days per test), so only one data set was collected in time for this paper, which limits our ability to do uncertainty quantification of the test data. Nonetheless, the model update process framework is able to incorporate new results as they become available. In a way, the dynamic update problem is similar to the static update problem just discussed with an added dimension in terms of frequency. This similarity is exploited to extend the MLS solution to dynamic problems where the FRF complex coefficients replace static displacements. Furthermore, parameters variations are conducted the same way as in the static case except that the uncertainty quantification for dynamics uses principal components bounds instead of variances.

Early in the development of the update algorithms, a decision was made to work with FRF data directly as opposed to parameters extracted from the FRF such as modal

frequency, damping, and mode shapes. Although this approach requires more data storage at any given time, during the uncertainty quantification phase there is no risk of improperly pairing extracted features when reconciling analysis and tests. For example, if modal frequencies and modes shapes are used, mapping of the measured and predicted values during update is a non-trivial task. Moreover, during parameter uncertainty propagation, one needs to ensure that the same mode and frequency is being observed. None of these issues are present when working directly with the FRF.

Principal components (PC) analysis provides the means to compare multi-input multi-output problems efficiently. To compute the principal components, the singular values of the frequency response function matrix at a particular frequency, sized q x r, are computed. For the case where $q > r$, the number of principal components is r. Analogous to principal strains or stresses in solid mechanics, these principal components correspond to the extreme values of the response. When comparing models, instead of comparing the FRF for a particular input/output pair, the principal components are compared instead. Although the results in the following show a comparison of minimum and maximum principal values, all FRF data is used internally for a qualitative assessment. Figure 14 shows a comparison of the MLS model (19 parameters, basis order 2, 300 NASTRAN solutions, and 801 frequency points) versus the finite element model (FEM) PC; crosses are for MLS predictions and dashed are for FEM. The MLS average error for this case is 7.1×10^{-5} m/N. With 18 outputs and 3 inputs, to verify that the FEM and the MLS models are in agreement, all 54 individual FRF would need to be examined, as compared to one PC plot in Figure 14.

The benefit of using principal components should be evident but their use is even more important during uncertainty quantification. For dynamic model updates, mode shapes and natural frequencies from NASTRAN solutions are assembled in MATLAB with 1 % modal damping to compute the predicted FRF. From 300 individual FRF, PC for each solution are computed as a function of frequency. By counting the number of times a particular value occur, the probability of observing a set (as a function of frequency) of PC values from a population of 300 is 1/300, however, the probability of observing a particular PC value at a certain frequency is $\geq 1/(300N_f)$, where N_f is defined in Eq. (2) as the number of spectral lines. For a population of FEM solutions, given that the parameters are varied over their prescribed bounds, the maximum and minimum PC bound can be computed at each frequency point, for single and multi-parameter variations, with probability $\geq 1/(NN_f)$, where N is the population size. If the test PC fall within the predicted PC bounds, then the probability of finding a set of parameters that captures the test response is also bounded and nonzero, i.e. a solution exist to predict the measure response.

After considering various parameter sets, the set chosen is shown in Table 2. With these parameters the PC bounds are computed and shown in Figure 15. Dashed lines correspond to test PC (maximum and minimum values) whereas solid corresponds to FEM PC bounds. This parameter set is chosen because the test PC are captured within the FEM PC bounds, indicating that there is a probability $\geq 4\times10^{-6}$ that a parameter set can be found to explain the measured response. If multiple tests FRF are at hand, the PC for

each case can be superimposed onto Figure 15 to assess the adequacy of the parameter selection. It is important to recognize that Figure 15 depicts in general the effects of parameter uncertainty in the FRF. Using the MLS model, the same PC analysis is conducted varying one parameter at a time while holding all other parameters at their nominal values to study the effect of the individual parameters. These results, although not shown, are also used to select the set shown in Table 2.

Another benefit of using principal components is for troubleshooting dynamic tests. Recall that the PC values can be thought off as the maximum and minimum system response due to a unit input. After examining Figure 15, the test engineer should realize that the excitation and/or measurements levels are drastically different in different directions. The problem arises when attempting to excite and observe the torus in-plane and out-of-plane modes. To solve this problem both the shaker and laser positioning would need to be corrected as well as the sensor range. Although efforts are underway to correct for test deficiencies, data from those tests are not available. Pre-test analysis results obtained after the initial tests corroborated our suspicions that there are an insufficient number of sensors to distinguish among different modes. This hinders our ability to use conventional orthogonality of test and analysis modes to compare models. Nonetheless, if all FRF are reconciled between test and analysis, and enough data is collected to discern differences in mode shapes, all the conventional correlation tools can be applied as a post-processing for linear model correlation.

To compare results before and after the dynamic update, Figure 16 shows the PC from the baseline NASTRAN model (including updated static parameters) and test. Table 3 shows the first 8 dominant frequencies corresponding to Figure 16. Although the magnitudes are reasonable, most resonant frequencies are shifted from test and analysis. Figure 17 shows the NASTRAN PC with dynamic parameter updates and Figure 18 shows parameter variations after optimization; black corresponds to parameters with decreased values and white are those with increased values. After this update, higher frequency modes improved significantly but low frequency modes are shifted. This low frequency shift is due to a slight mass change not constrained in the optimization step. Also Table 3 shows a comparison of the first eight dominant frequencies before and after optimization, showing a significant improvement in some of the high frequency modes. Examining the actual parameter changes, note that several parameters are nearly unchanged while others are at their extreme values. Often this would be a cause for concern but remember that parameter bounds are defined such that any value is equally probable, hence, from an engineering viewpoint acceptable. Furthermore, updated parameters after dynamic updates could impact the static solution. This is in fact the case but in this example the impact is small compared to the problem uncertainty. Although an optimum parameter solution set is shown for one complete update cycle using both static and dynamic data, this is only one possible parameter set. Uncertainty quantification of the measured data needs to be examined and the process repeated until all the observed data is explained by our model

Finally, the last issue not mentioned thus far is the effect of extrapolation errors in the solution because MLS is used instead of NASTRAN. Results have been shown using

both NASTRAN and MLS predictions but the optimum solution set is determined using MLS only. Errors associated with differences between MLS and NASTRAN predictions will impact our predictive accuracy and the optimum parameter set values. To refine the parameter solution, one should compute more high fidelity NASTRAN solutions near the optimum set. However, the investment in using high fidelity solutions must be traded against remaining experimental and parameter uncertainty. At this point, efforts are underway to quantify experimental uncertainty.

Concluding Remarks

A procedure to conduct static and dynamic parameter updates of finite element models has been developed and demonstrated that integrates analysis of variance and principal components. Analysis of variance and confidence intervals are used to bound the response uncertainty for static problems, but for dynamics principal components are used to assess uncertainty bounds. These bounds establish the probability of finding a solution that reconciles test with analysis results. In the formulation, a Moving Least Squares (MLS) response surface model is created and used to capture expensive time-consuming high fidelity structural solutions into models for optimization, analysis of variance, and principal component analysis. For parameter selection, analysis of variance is the primary tool used with static problems and principal components of the frequency responses are used for dynamic problems. By using MLS a relatively small number of high fidelity solutions are needed to construct the response surface model used in all subsequent analysis. In fact, MLS models enable the use of exhaustive optimization searches like those required by genetic algorithms; otherwise it would be impractical to use genetic algorithms with high fidelity models.

For the hexapod torus demonstration problem, correlation of static displacements between test and analysis is improved to the point where the majority of the measured points are within the measurement uncertainty for 19 out of 21 measured outputs. Starting from the updated static solution, frequency response functions from 18 sensors and 3 excitation sources are used to reconcile test and analysis. An initial comparison of the dominant frequencies before and after the update shows that five 5 out of 8 frequencies are significantly improved. However, problems with the dynamic test setup hindered a full comparison of mode shapes at this time.

Although finding a parameter set that reconciles the FEM with test is the ultimate goal from an engineering viewpoint, the true value of the work is in the uncertainty quantification and confidence interval calculations. A particular solution, like the one presented, is one of many possibilities. For the solution to be more meaningful, tighter probability statements would have to be computed.

Acknowledgements

The authors are grateful to Dr. Thiagaraja Krishnamurthy at NASA Langley for providing the FORTRAN code that is the basis for the newly developed Moving Least Squares response surface MATLAB script files. Not only was he invaluable in getting the software to work but he also provided the examples used to verify the solutions.

Also, we would like to thank Dr. Luis Crespo and Dr. Sean Kenny for insightful discussions on sampling approaches and optimization.

References

1. *Avitabile, P.*: "Model Updating- Endless Possibilities." Proceedings of the 18th International Modal Analysis Conference, San Antonio, TX, Feb. 2000, pp. 562-570.
2. *Friswell*, M.I., and Mottershead, J.E.: Finite Element Model Updating in Structural Dynamics, Kluwer Academic Press, Dordrecht, 1995.
3. Hasselman, T.K., Chrostowski, J.D., and Ross, T.J.: "Propagation of Modeling Uncertainty Through Structural Dynamic Models," Proceedings of the 35th AIAA/ ASME/ASCE/AHS/ASC Structures, Structural Dynamics, and Materials Conference, 1994, Paper No. AIAA 94-1316, SC.
4. Herendeen, D.L., Woo, L., Hassleman, T.K., and Zimmerman, D.C.: "Analysis-Test Correlation and Model Updating of Dynamic Systems Using MDO Software Tools," Proceedings of the 7th AIAA/USAF/NASA/SSMO Symposium on Multidisciplinary Analysis and Optimization, 1998, Paper No. 98-4730, St. Louis, MO.
5. *Alvin*, K.F.: "Finite Element Model Update via Bayesian Estimation and Minimization of Weighted Residuals," AIAA Journal, Vol. 35, No. 5, 1997.
6. *Farhat*, C. and Hemez, F.M.: "Updating Finite Element Dynamic Models Using an Element-by-Element Sensitivity Methodology," AIAA Journal, Vol. 31, No. 9, 1993, pp. 1702-1711.
7. *Montgomery D.*C., Design and Analysis of Experiments, John Wiley & Sons, New York, 5th ed. 2001
8. *Uebelhart, S.*A., Miller, D.W., and Blaurock, C.: "Uncertainty Characterization in Integrated Modeling." Proceedings of the 46th AIAA/ASME/ASCE/AHS/ASC Structures, Structural Dynamics, & Materials Conference, April 2005, Austin TX., AIAA 2005-2142.
9. *Oberkampf, W.*L., Trucano, T.G., and Hirsch, C.: "Verification, Validation, and Predictive Capability in Computational Engineering and Physics." SAND 2003-3769, Feb. 2003.
10. *Roach, P.*P., Verification and Validation in Computational Science and Engineering, Hermosa Publishers, Albuquerque, NM, 1998.
11. *Thacker, B.*H.: "The Role of Nondeterminism in Computational Model Verification and Validation." Proceedings of the 46th AIAA/ASME/ASCE/AHS/ASC Structures, Structural Dynamics, & Materials Conference, April 2005, Austin TX, AIAA 2005-1902.
12. *Krishnamurthy*, T. and Romero, V.J.: "Construction of Response Surface with Higher Order Continuity and its Application to Reliability Engineering." Proceedings of the *43rd AIAA/ASME/ASCE/AHS/ASC Structures, Structural Dynamics, and Materials Conference,* April 22-25, 2002, Denver, CO, AIAA Paper No. 2002-1466.
13. *Zhang, L.*, Fei, Q., and Guo, Q.: "Dynamic Finite Element Updating Using Meta-Model and Genetic Algorithm," Proceedings of the IMAC-XXIII conference, Orlando FL, 2005.
14. *Hasselman T.*, Yap K., Yan H. and Parret, A.: "Statistical Energy Analysis by Principal Components for Mid-Frequency Analysis." Proceedings of the 43rd

AIAA/ASME/ASCE/AHS/ASC Structures, Structural Dynamics, and Materials Conference, April 2002, Denver, CO. AIAA 2002-1395.
15. *Chipperfield, A., Fleming, P. J., Pohlheim, H. and Fonseca, C. M.*: "Genetic Algorithm Toolbox for use with Matlab." Technical Report No. 512, Department of Automatic Control and Systems Engineering, University of Sheffield, 1994.
16. *Hammersley*, J.M.: "Monte Carlo methods for solving multivariable problems." Proceedings of the New York Academy of Science, Vol. 86, 1960, pages 844-874.
17. *Berger*, K.T., Horta, L.G., Taleghani, T.K: "Static Testing of an Inflatable/Rigidizable Hexapod Structure." Proceedings of the 45th AIAA/ASME/ASCE/AHS/ASC Structures, Structural Dynamics, and Materials Conference, Palm Springs, CA, April 2004, AIAA-2004-1801
18. *Adetona* O., Horta, L.G., Taleghani, B.K., Blandino, J.R., and Woods, K.J.: "Vibration Studies of an Inflatable/Rigidizable Hexapod Structure with a Tensioned Membrane." Proceedings of the 44th AIAA/ASME/ASCE/AHS Structures, Structural Dynamics, and Materials Conference, AIAA Paper No. 2003-1737, April 2003, Norfolk VA.
19. *Vinson*, J.R. and Sierakowski, R.L.: The Behavior of Structures Composed of Composite Materials, Martinus Nijhoff, Dordrecht, The Netherlands: 1989.

Table 1. Parameter Nominal and Updated values from static tests

No.	Parameter Description	Nominal Values	Updated Values
1	Tube E1,E2 (N/m^2)	5.4217e+010	3.8000e+010
2	Tube shear 25 (N/m^2)	2.1578e+009	1.8997e+009
3	Tube shear 26 ((N/m^2)	2.1578e+009	2.361e+009
4	Tube shear 27 (N/m^2)	2.1578e+009	1.5100e+009
5	Tube shear 26 (N/m^2)	2.1578e+009	2.3686e+009
6	Tube shear 28 (N/m^2)	2.1578e+009	1.8495e+009
7	Tube shear 29 (N/m^2)	2.1578e+009	1.5919e+009
8	Tube shear 30 (N/m^2)	2.1578e+009	1.7473e+009
9	Tube shear 31 (N/m^2)	2.1578e+009	1.5234e+009
10	Tube shear 32 (N/m^2)	2.1578e+009	2.3162e+009
11	Tube shear 33 (N/m^2)	2.1578e+009	1.5100e+009
12	Tube shear 34 (N/m^2)	2.1578e+009	2.1607e+009
13	Tube shear 35 (N/m^2)	2.1578e+009	1.8155e+009
14	Joint E (N/m^2)	3.033e+009	2.1200e+009
15	Tube thickness 24 (m)	0.000356	0.000415
16	Tube thickness 25 (m)	0.000356	0.000375
17	Tube thickness 34 (m)	0.000356	0.000426
18	Tube thickness 35 (m)	0.000356	0.000411

Table 2. Parameter Nominal and Updated values from dynamic tests

No.	Parameter Description	Nominal Values	Updated Values
1	Stiffness K2 (*N/m*)	3667.2	3563.6
2	Stiffness K1 (*N/m*)	3745	3715.1
3	Stiffness K3 (*N/m*)	3726	3694.6
4	Tube Density Mat8 10 (kg/m^3)	1765	1466.6
5	Joint Density Mat 2 (kg/m^3)	1346.6	1456.7
6	Joint Density Mat 5 (kg/m^3)	1346.6	1348.6
7	Joint Density Mat 6 (kg/m^3)	1346.6	1427.9
8	Joint Density Mat 7 (kg/m^3)	1346.6	1343.6
9	Joint Density Mat 8 (kg/m^3)	1346.6	1405
10	Joint Density Mat 9 (kg/m^3)	1346.6	1251.3
11	Joint Density Mat 11 (kg/m^3)	1346.6	1264
12	Joint Density Mat 12 (kg/m^3)	1346.6	1193.3
13	Joint Density Mat 13 (kg/m^3)	1346.6	1305.8
14	Joint Density Mat 14 (kg/m^3)	1346.6	1271.6
15	Joint Density Mat 15 (kg/m^3)	1346.6	1374.2
16	Joint Density Mat 16 (kg/m^3)	1346.6	1156.8
17	Joint thickness 4 (*m*)	0.00317	0.00291
18	Joint thickness 8 (*m*)	0.00634	0.00576
19	Flange thickness 1 (*m*)	0.01016	0.00817

Table 3. Comparison of the first eight peak frequencies shown for test, nominal, and update model

Test Frequencies (Hz)	Nominal Model Frequencies (Hz)	Updated Model Frequencies (Hz)
4.32	4.31	4.59
4.63	4.61	4.97
14.55	12.59	13.47
18.75	17.59	18.75
37.13	35.01	37.13
49.60	45.52	48.71
65.66	61.36	65.66
83.08	81.96	80.89

Figure 1 – TSU Hexapod structure

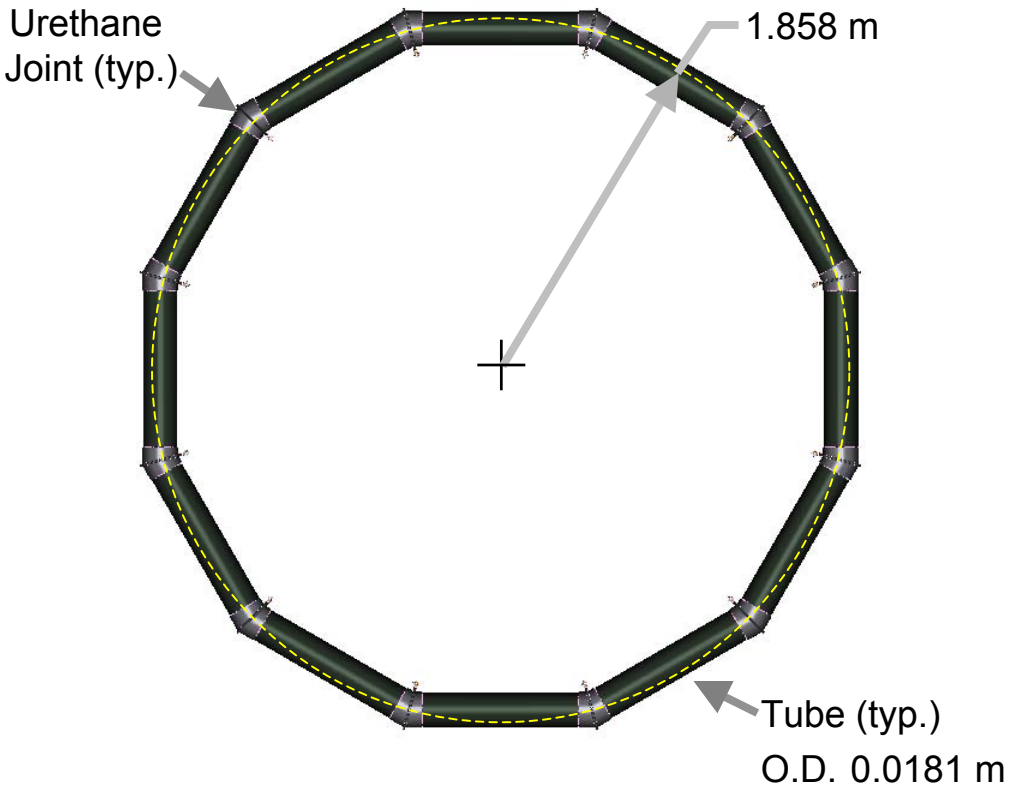

Figure 2 – Torus test article

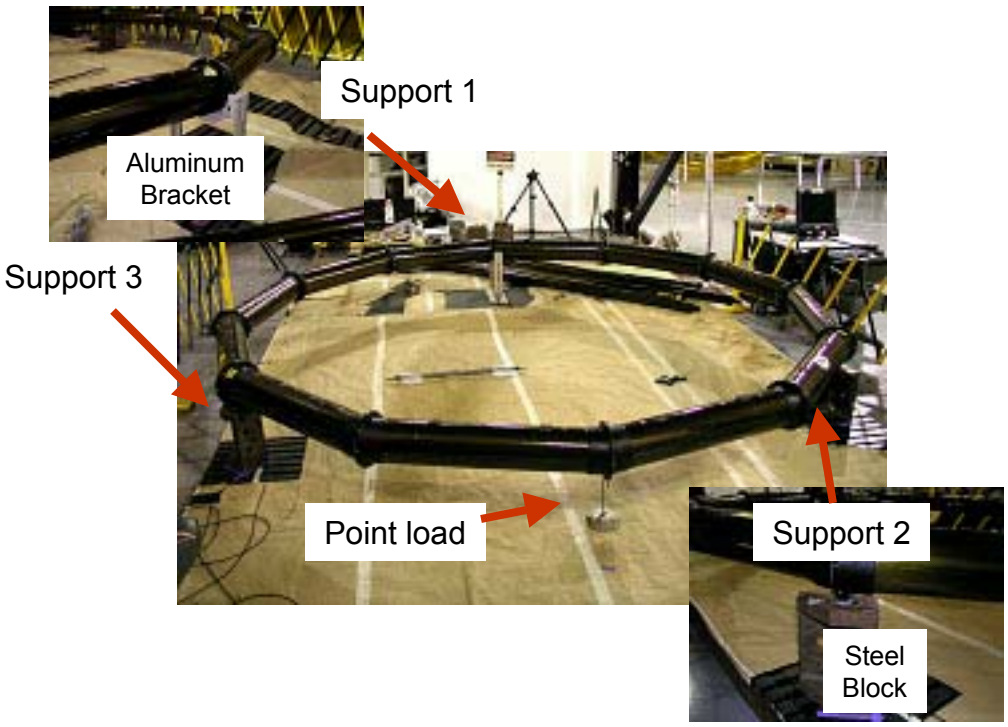

Figure 3 – Torus static test configuration

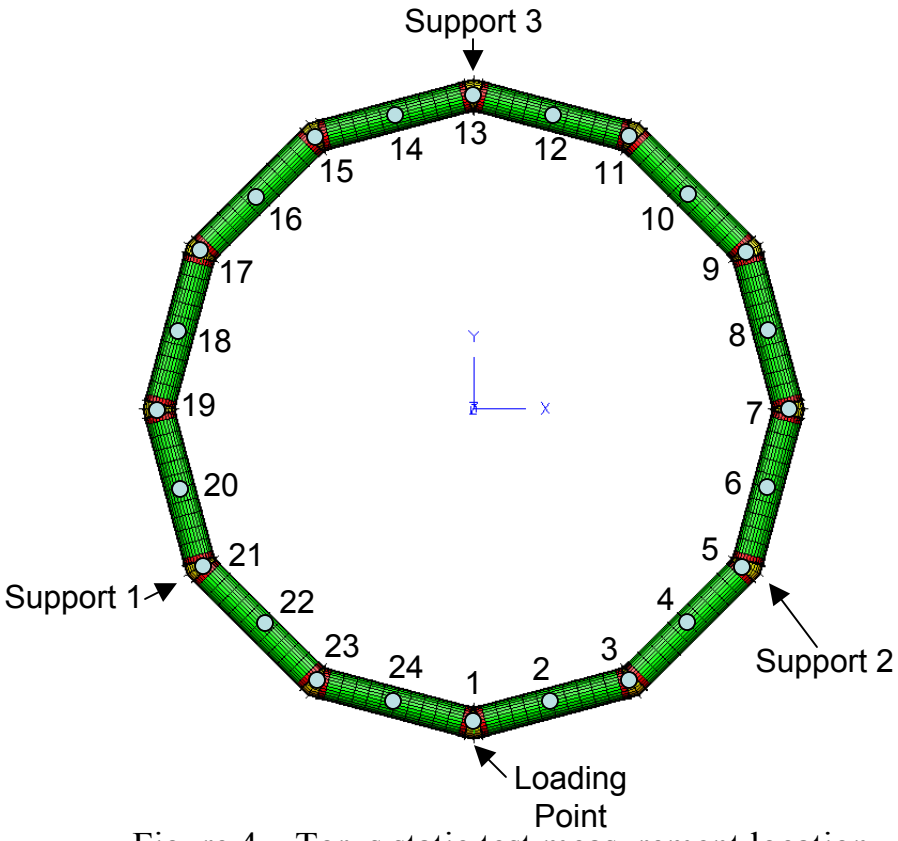

Figure 4 – Torus static test measurement location

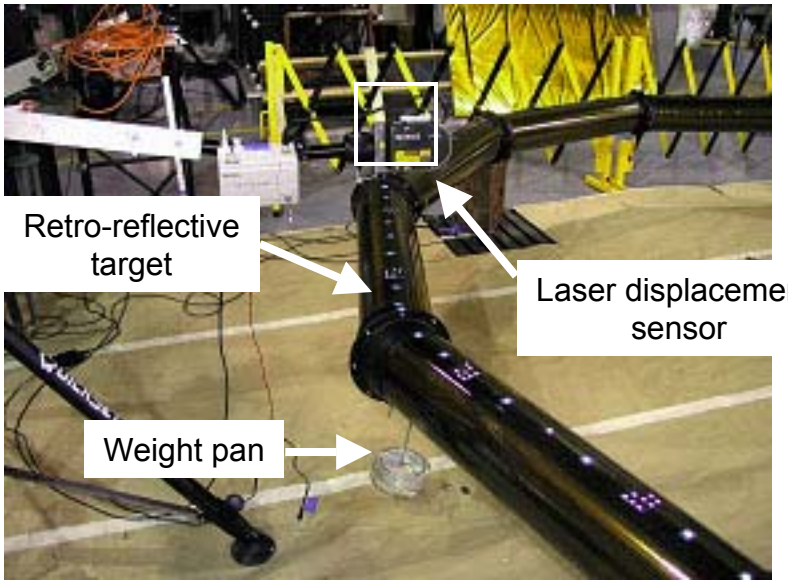

Figure 5 – Torus static test measurement location

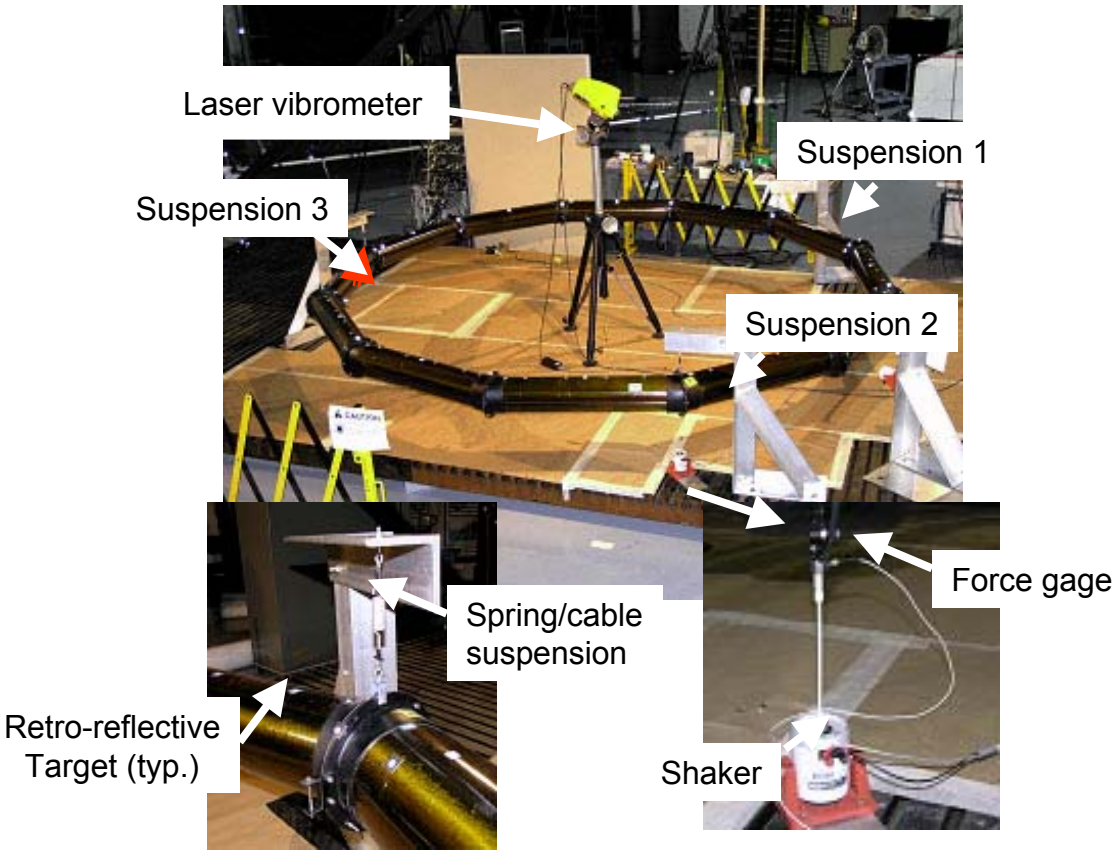

Figure 6 – Torus dynamic test suspended configuration

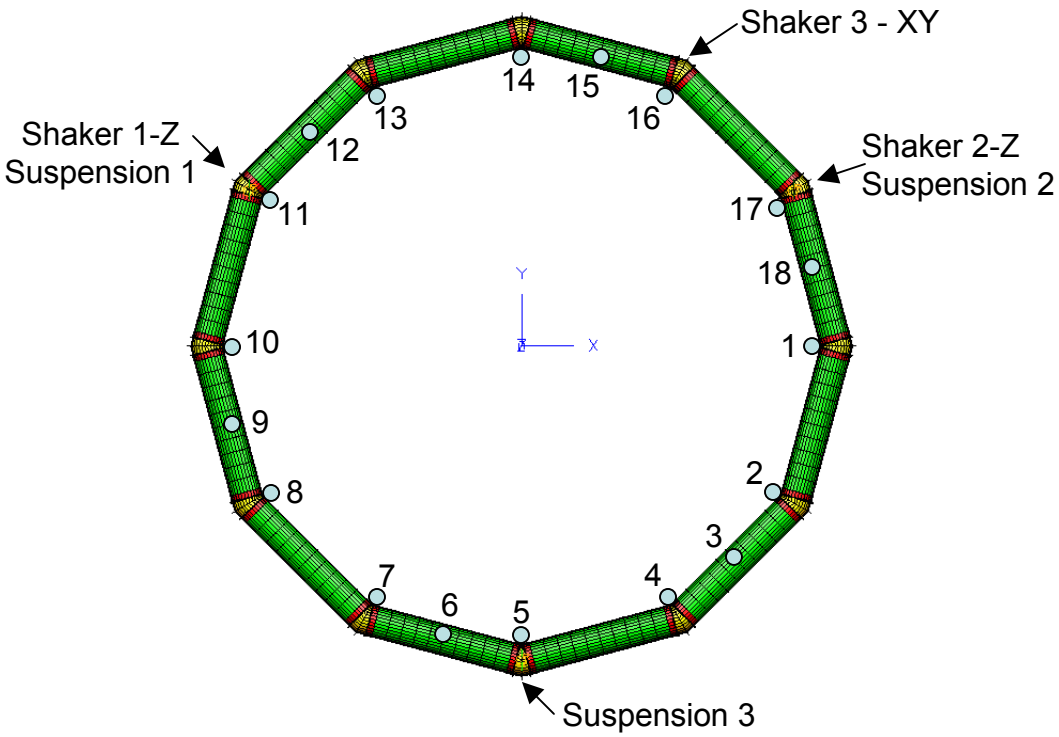

Figure 7 – Dynamic test measurement and input locations

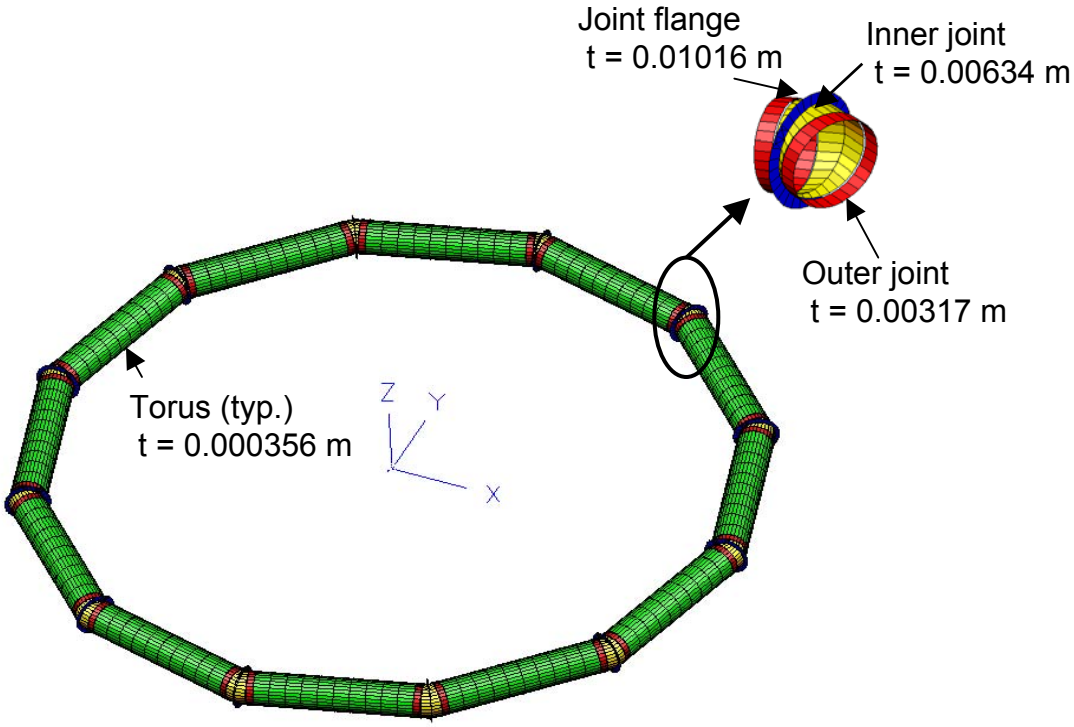

Figure 8 – Torus finite element model mesh with baseline plate thicknesses

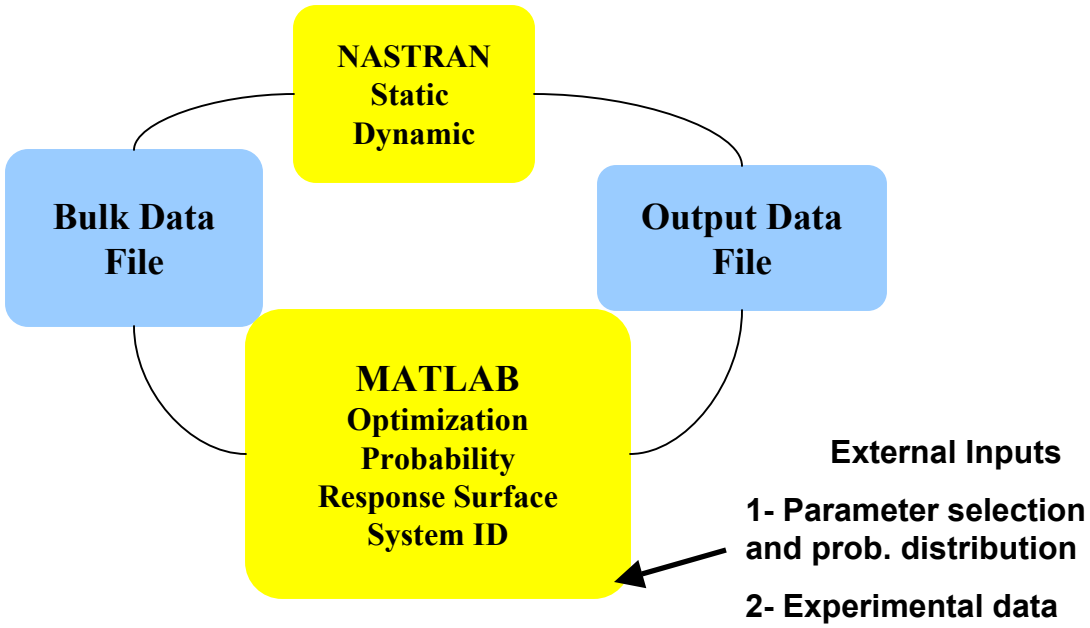

Figure 9 Schematic of computational framework

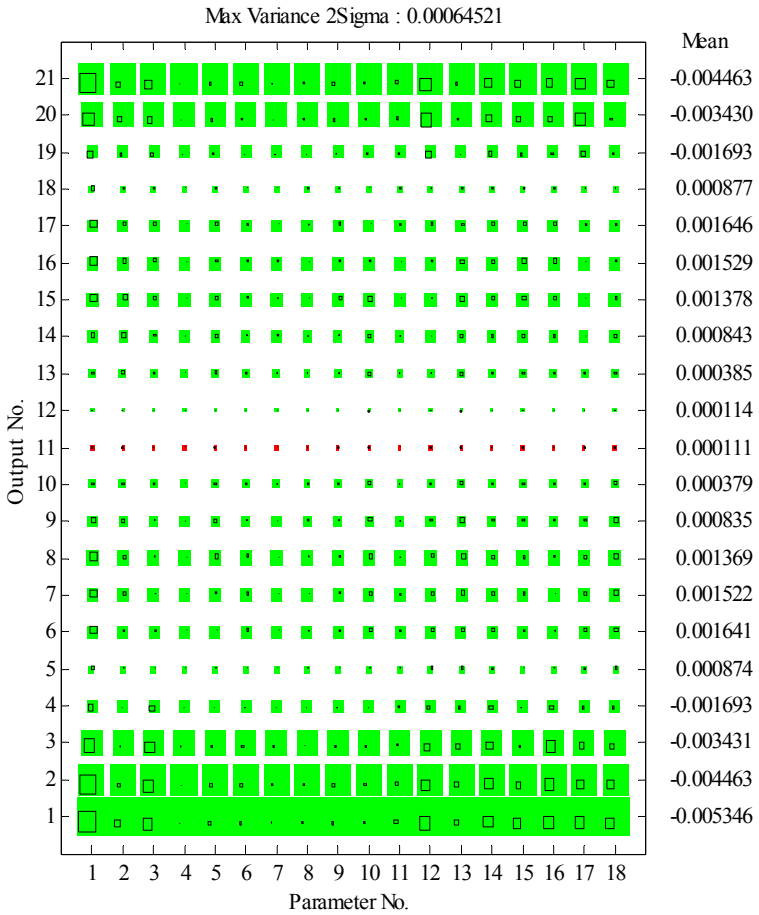

Figure 10 – Analysis of output variance

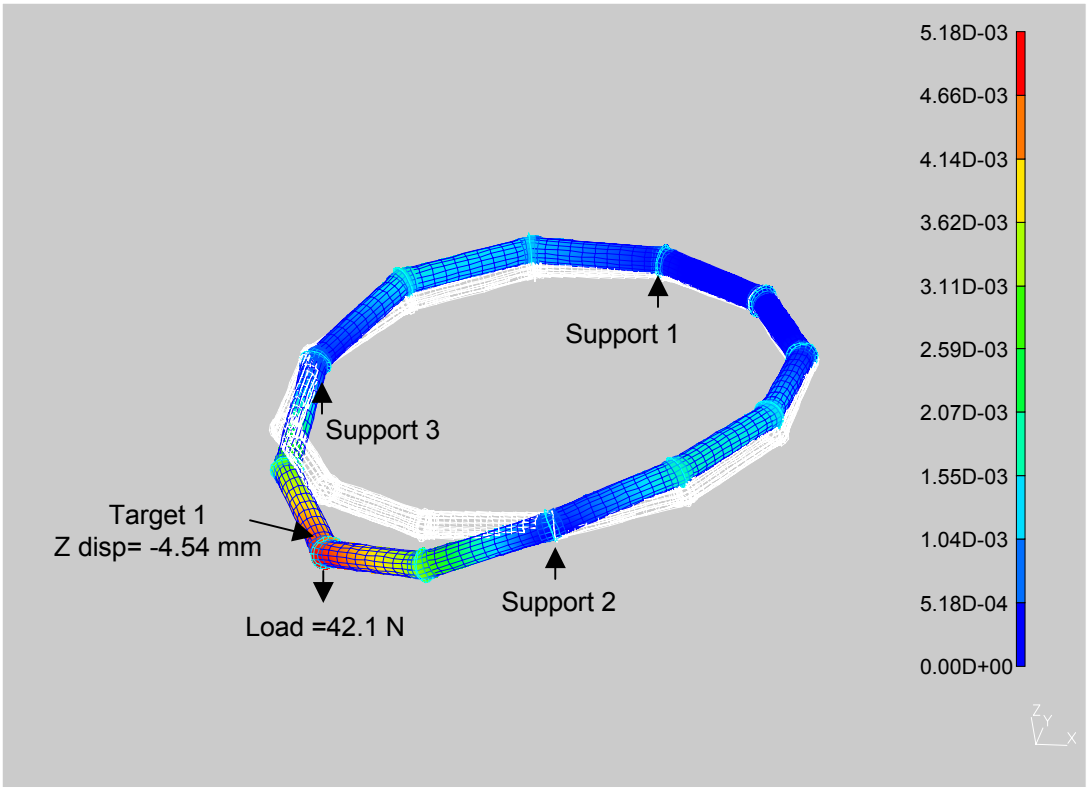

Figure 11 – Baseline torus FEM static deflections

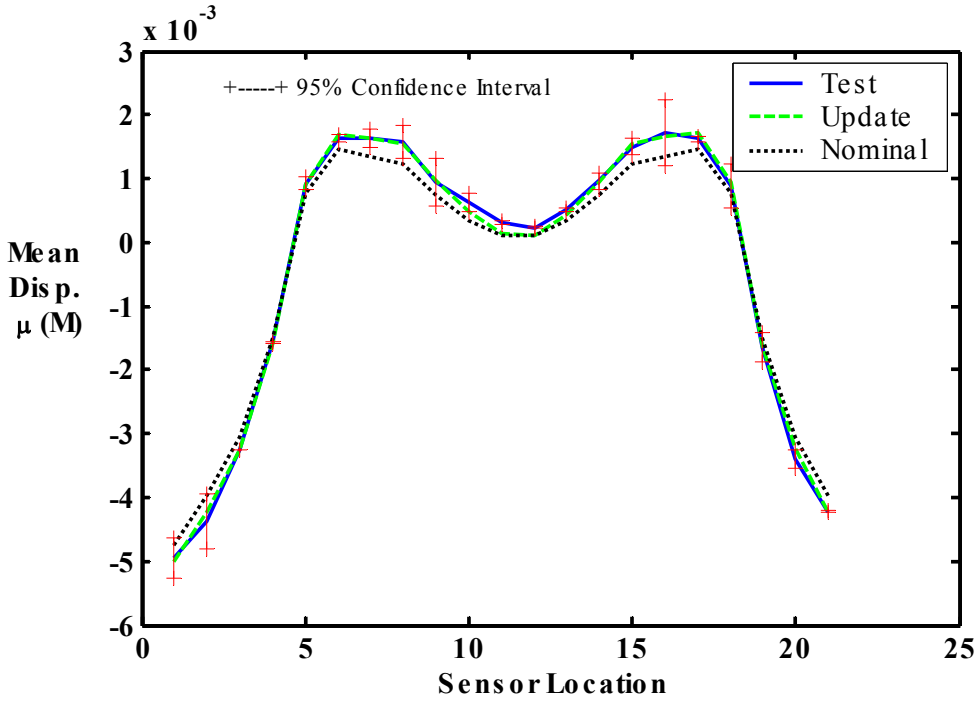

Figure 12 – Torus static deformation results for test, baseline FEM and updated FEM analysis

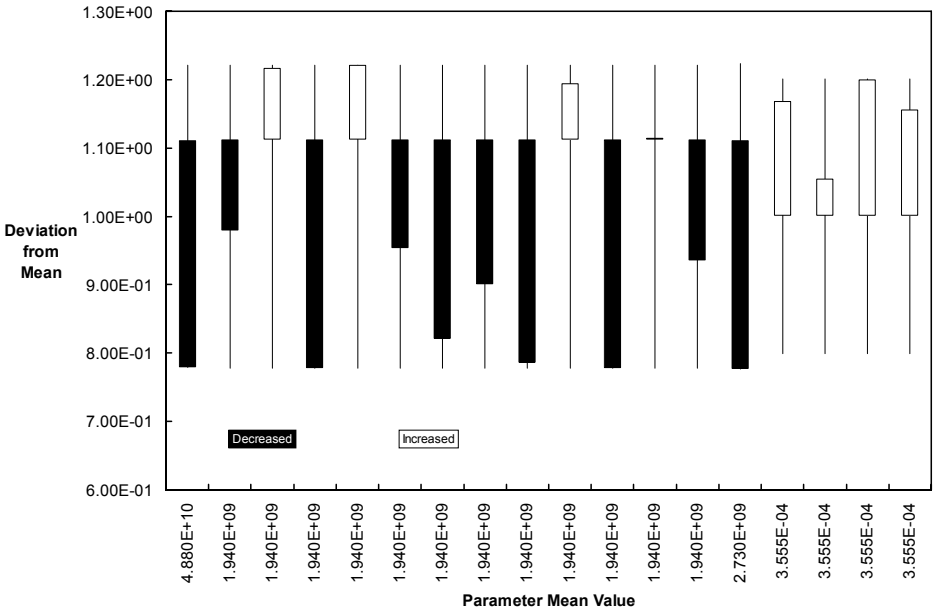

Figure 13. Summary of parameter changes for static problem

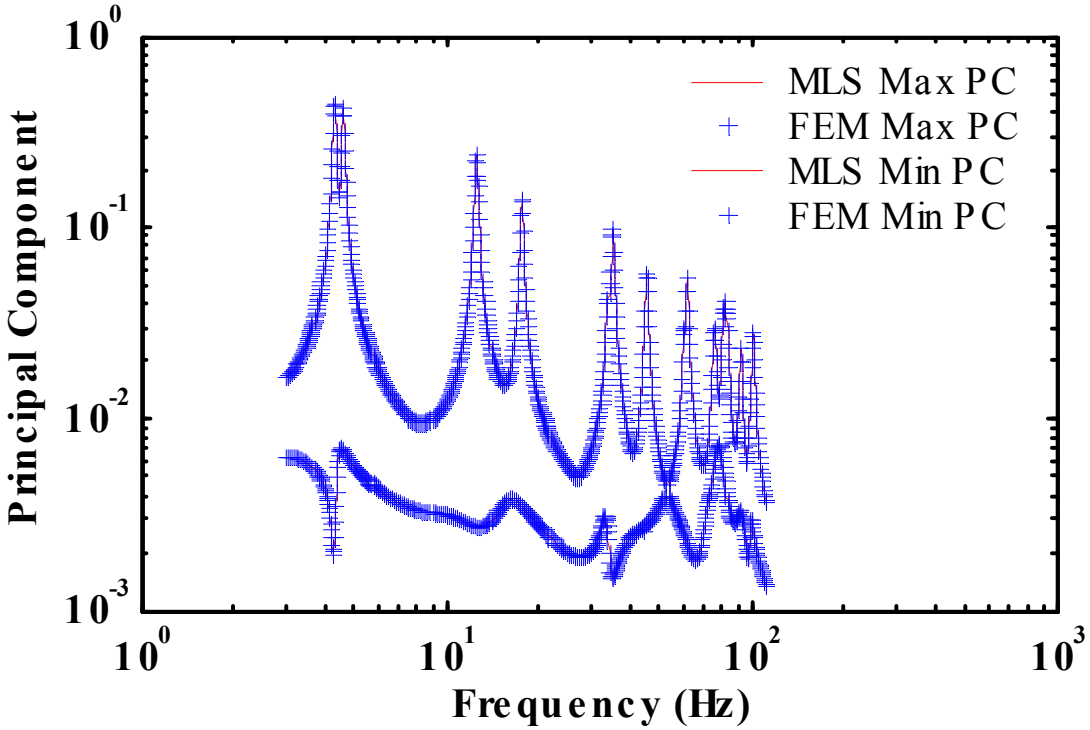

Figure 14. Comparison of principal components for MLS model and FEM

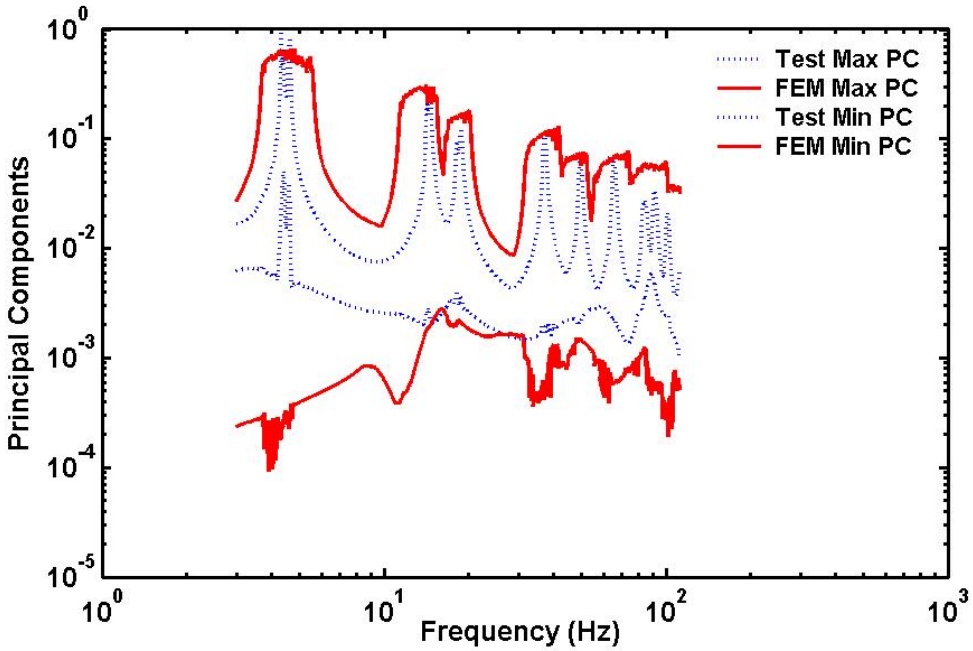

Figure 15. Principal component bounds with probability greater than 4e-06

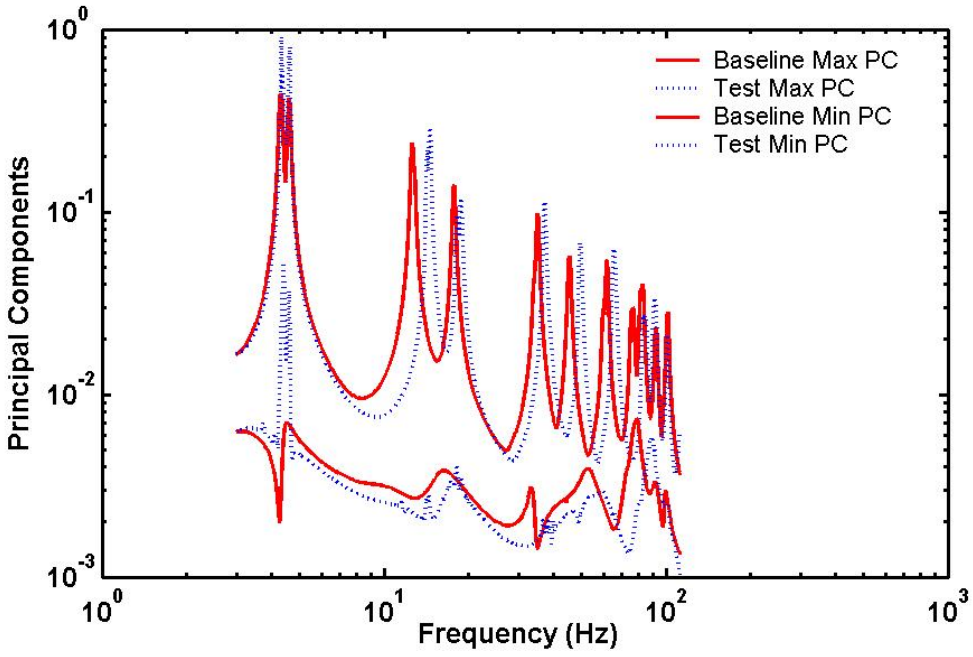

Figure 16. Comparison of Principal components for nominal solution and test

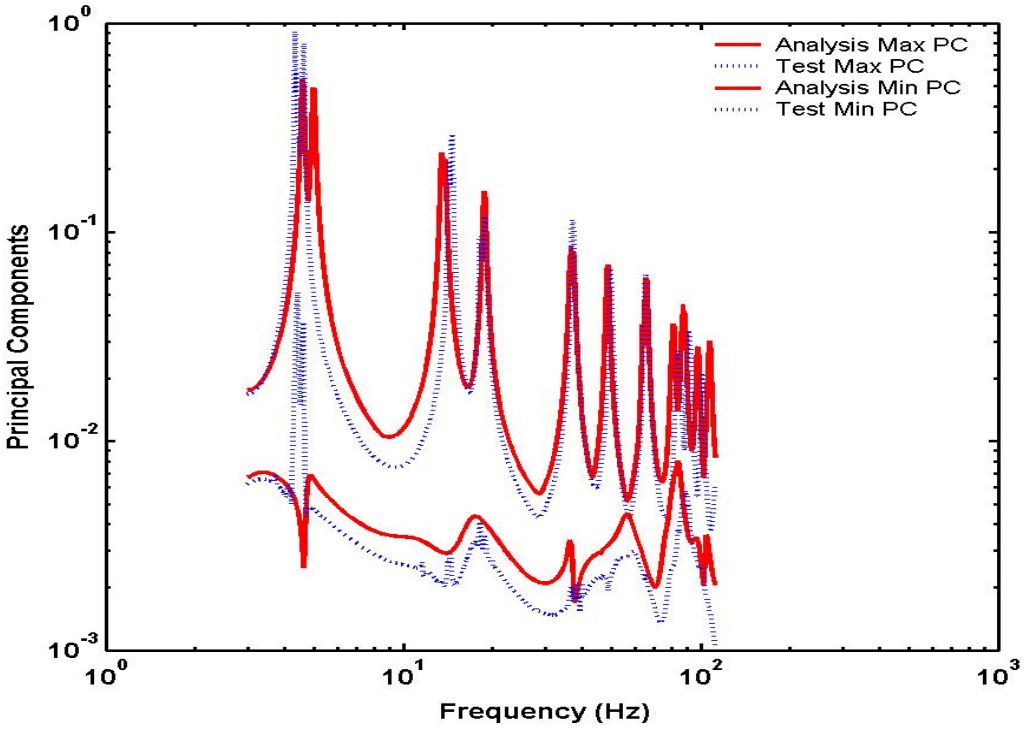

Figure 17. Comparison of principal components for test and optimized solution

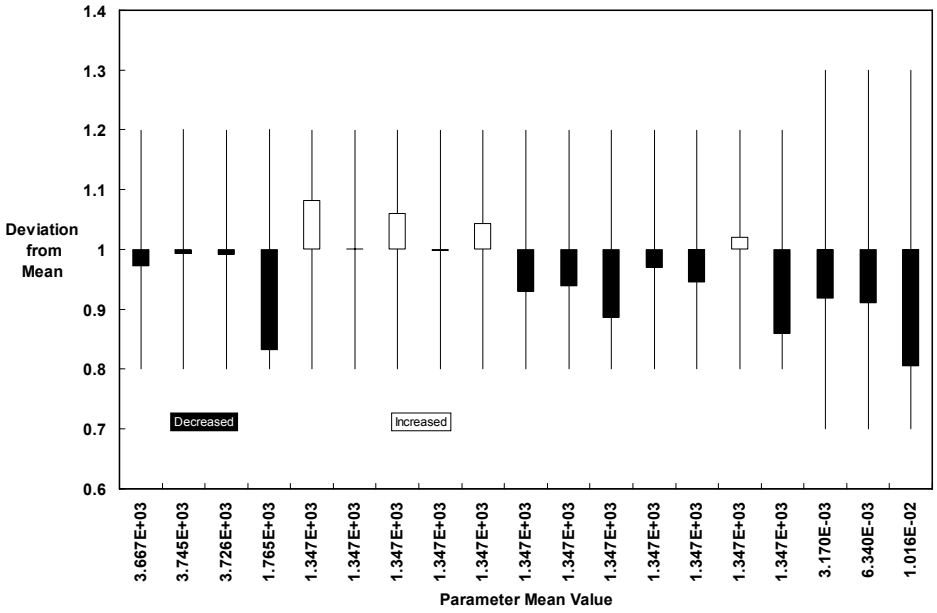

Figure 18. Summary of parameter changes for dynamic solution